FULL PAPER

Self-Assembling Prodrugs by Precise Programming of Molecular Structures that Contribute Distinct Stability, Pharmacokinetics, and Antitumor Efficacy

Hangxiang Wang, Haiyang Xie, Jianguo Wang, Jiaping Wu, Xueji Ma, Lingling Li, Xuyong Wei, Qi Ling, Penghong Song, Lin Zhou, Xiao Xu, and Shusen Zheng**

The availability of precisely modulated chemical modifications dramatically affects the physicochemical properties of pristine drugs and should facilitate the amphiphilic self-assembly of prodrugs into supramolecular nanoprodrugs (SNPs). However, rationally designing such prodrugs to achieve favorable clinical outcomes still remains a challenge. Here, a library of prodrugs through site-specific attachment of a variety of lipophilic moieties to the antitumor agent SN-38 (7-ethyl-10-hydroxycamptothecin) is constructed. Taking advantage of the role of hydroxyl groups as solvophilic moieties, these prodrugs exhibit self-assembly in aqueous environments, allowing for the identification of five prodrugs capable of self-assembling into SNPs at high drug concentrations. Importantly, in vivo studies demonstrate that the antitumor activity of the SNPs correlates well with their stability and long-term circulation. In addition, the modular feature of this SNP design strategy offers the opportunity to readily incorporate additional valuable functionalities (e.g., tumor-specific targeting ligands) to the particle surface, which is further exploited to improve antitumor efficacy in mouse xenograft models. Thus, this structure-based reconstruction of SN-38 molecules significantly improves the potency of SNPs for clinical use. These results also provide novel mechanistic insights into the rational design of prodrugs.

1. Introduction

Efficient delivery of therapeutic agents with high tissue-targeting ability is urgently needed for the treatment of numerous disorders including cancers.[1–3] Over the past two decades, a myriad of nanoscale vehicles have been developed for delivering high payloads of hydrophobic agents to tumors because these nanovehicles preferentially accumulate within solid tumors through the enhanced permeability and retention (EPR) effect.[4] Traditional formulation of these hydrophobic therapeutics has included coprecipitation with amphiphilic block copolymers,[5–8] modification with large hydrophilic moieties,[9,10] and complexation within a molecular container.[11,12] These delivery methods are undoubtedly effective and several of them are currently under development in clinical trials.[7,13] However, most of these methods require a large quantity of adjuvant materials and complicated processes for drug fabrication, which could lead to significantly lower drug payloads or cause unnecessary side effects.

Amphiphilic self-assembly of pure prodrugs into nanoscale vehicles through precisely modulating the chemical structures of pristine drugs is attractive. Indeed, a few notable methods have been explored for this purpose, including the following: i) the use of squalene, a natural hydrophobic compound, to covalently couple with hydrophilic antitumor drugs (i.e., gemcitabine[14] and doxorubicin[15] and ii) the conjugation of an oligo(ethylene glycol) with hydrophobic drugs to form amphiphilic constructs.[16–18] These strategies utilize drugs themselves as hydrophilic or hydrophobic moieties, respectively, to reconstruct new small-molecule amphiphiles. The resultant prodrugs can self-assemble in aqueous media into supramolecular nanoarchitectures that are capable of releasing pharmacologically active molecules in response to endogenous stimuli upon systemic administration.[19–21] Obviously, compared with polymeric assembly-based delivery counterparts, the methods using small-molecule prodrugs and self-assemblies have their own niche in high drug loading, simple syntheses, and economical fabrication processes. Despite several recent advances in

Dr. H. Wang, H. Xie, J. Wang, J. Wu, L. Li, Dr. X. Wei, Dr. Q. Ling, Dr. P. Song, Dr. L. Zhou, Prof. X. Xu, Prof. S. Zheng
The First Affiliated Hospital
School of Medicine
Key Laboratory of Combined Multi-organ Transplantation
Ministry of Public Health
Key Laboratory of Organ Transplantation
Collaborative Innovation Center for Diagnosis and Treatment of Infectious Diseases
Zhejiang University
Zhejiang Province
Hangzhou 310003, P. R. China
E-mail: zjxu@zju.edu.cn; shusenzheng@zju.edu.cn
Dr. X. Ma
Department of Chemistry
Zhejiang University
Xixi Campus, Hangzhou 310028, P. R. China

DOI: 10.1002/adfm.201501953

bottom-up approaches for nanoprodrug fabrication,[22] little is known about the structure–activity relationship. This knowledge gap could greatly limit the further rational design of prodrug-based platforms. Thus, the continuing improvements and understanding of design strategies are highly desirable for future clinical translation.

SN-38 (7-ethyl-10-hydroxycamptothecin) is a potent inhibitor that targets DNA topoisomerase I and inhibits cell growth, particularly in rapidly proliferating cells.[23] Unfortunately, SN-38 is neither compatible with conventional polymeric delivery materials (e.g., poly(ethylene glycol)-*block*-poly(D,L-lactic acid)) nor dissolvable in pharmaceutically acceptable solvent systems (e.g., Tween 80). Its derivative irinotecan (CPT-11), a water-soluble prodrug, was approved for clinical applications nearly 20 years ago. However, the major drawback of CPT-11 use is its inefficient conversion to the active metabolite SN-38 by carboxylesterases.[24] In addition, CPT-11 elicits severe diarrhoea, which prevents dose intensification and limits efficacy.[25] We recently demonstrated that appropriate molecular engineering could make SN-38 suitable for incorporation into favorable copolymer-based delivery platforms, significantly improving the antitumor efficacy compared to CPT-11.[26] In preparing these prodrug-encapsulated nanoparticles, we noticed that several prodrugs have the tendency to form nanoaggregates rather than precipitates even in the absence of polymer materials and in spite of their largely hydrophobic nature.

In this work, we hypothesize that tethering SN-38 to a lipophilic tail could induce self-assembly in aqueous solutions by exploiting the role of 20 (or 10)-hydroxyl as a weakly polar moiety (**Figure 1**). Importantly, we demonstrate how structural variations in the hydrophobicity of modifiers confer distinct pharmacokinetic properties of the generated supramolecular nanoprodrugs (SNPs) and their potential clinical outcomes. Furthermore, due to the modular feature of designing strategy, we demonstrate that additional functionalities (e.g., tumor specific ligands) can be readily incorporated into these delivery SNPs in a coassembly manner for improving in vivo antitumor efficacy.

2. Results and Discussion

2.1. Prodrug Design and Self-Assembly of Prodrugs in Water

To test our hypothesis, we constructed a library of novel SN-38 derivatives wherein the 10 (or 20)-hydroxyl groups are functionalized by a variety of hydrophobic moieties (see the full compound list in Figure S1, Supporting Information).

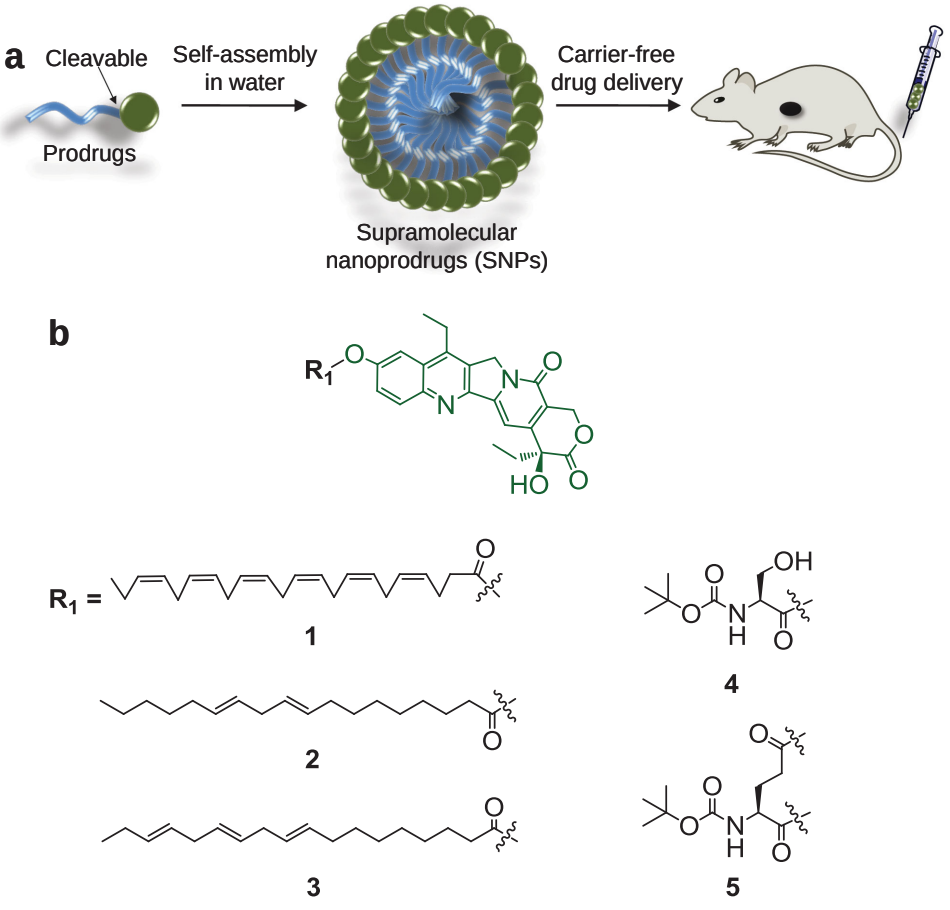

Figure 1. a) Rational molecular engineering of SN-38 to induce self-assembly in aqueous media for in vivo drug delivery. b) The molecular structures of prodrugs **1–5** were identified and optimized based on their self-assembly and solubility in water.

The chemistry used to modify the hydroxyl groups on SN-38 included the adaptation of ester and silyl ether chemistries. Hydrolytic cleavage of these two types of bonds in aqueous solutions could lead to the liberation of pharmacologically active SN-38 molecules. Specifically, altering the substituent on the silicon atom in silyl ethers could modulate hydrolysis rates,[27,28] thus providing the potential for controlled drug release at desirable acidic tumor site(s). Based on this rationale, the corresponding prodrugs **1–26** were synthesized without tedious synthetic effort using commercially available materials.

To evaluate the ability of prodrugs **1–26** to self-assemble in aqueous media, a simple reprecipitation method was exploited by rapid injection of prodrugs in dimethyl sulfoxide (DMSO) into an antisolvent (e.g., water) to form nanostructures.[29,30] Initially, the 10-hydroxyl groups of derivatives **6–8** were tethered with saturated fatty acids with varying alkyl chains and tested. However, injection of these compounds into water immediately induced precipitation rather than the formation of transparent solutions. In addition, Boc-protected amino acid-derived prodrugs **4**, **5**, and **11–16** were verified in terms of their self-assembly because our previous study showed that they readily coassemble with amphiphilic block copolymers.[26] As a result, this effort afforded two prodrugs, **4** and **5** (a structural analogue to a previously reported SN-38 dimer)[30] that are capable of dissolving in water. Very interestingly, in a comparison of polyunsaturated and saturated alkyl chains, we found that modification of the prodrugs **1**, **2**, and **3** with the polyunsaturated fatty acids docosahexaenoic acid, linoleic acid (LA), and α-linolenic acid, respectively, made them more amenable to assembly than when modified with saturated alkyl chains. We might attribute this result to the sufficient structural flexibility conferred by polyunsaturated alkyl chains, which can take an enthalpic gain as a consequence of their flexible structures and possible intermolecular π–π stacking.[31] In addition, strong π–π stacking between planar structures of SN-38 molecules could be considered. Although the prodrugs **22**, **23**, and **24**, whose phenolate groups were modified via the silyl ether bonds, also assembled in aqueous solutions, their rapid hydrolytic properties unfortunately made the nanostructures unstable, resulting in precipitation within 1 h.

To gain insight into the molecular mechanism of self-assembly, the prodrugs **25** and **26**, whose 20-hydroxyl groups instead of 10-hydroxyl groups were shielded by lipophilic tails, were synthesized, and their abilities to self-assemble were tested. These compounds failed to assemble and instead resulted in large precipitates. This instability is attributed to the relatively strong polarity of unshielded phenolate groups on SN-38. These results clearly supported the idea that the 20-hydroxyl group plays a vital role as a weakly polar (solvophilic) moiety in stabilizing assembly. Thus, the self-assembly of SN-38 prodrugs can be finely tailored by exploiting structurally distinct modifications. Through systemic screening, we identified assembled SNPs for prodrugs **1–5** (termed SNPs **1–5**, respectively) that exhibited greater stability and higher solubility than the other molecules in aqueous media without the use of adjuvant materials (Figure 1b). The drug loadings of SNPs **1–5** were considerably high at 55.8, 59.9, 60.1, 67.7, and 78.8 wt%, respectively.

2.2. Characterization of Prodrug-Assembled SNPs

After injection into aqueous solution, an aliquot of the assembled nanoparticles was subjected to transmission electron microscopy (TEM). The prodrugs **1–5** exclusively formed uniform spherical shapes with extremely small diameters (close to 40 nm) (**Figure 2**c–g). Scanning electron microscopy (SEM) images also revealed the successful fabrication of prodrug-containing nanoparticles (Figure 2c–g, insets). Dynamic light scattering (DLS) analysis indicated that SNPs **1–5** have average

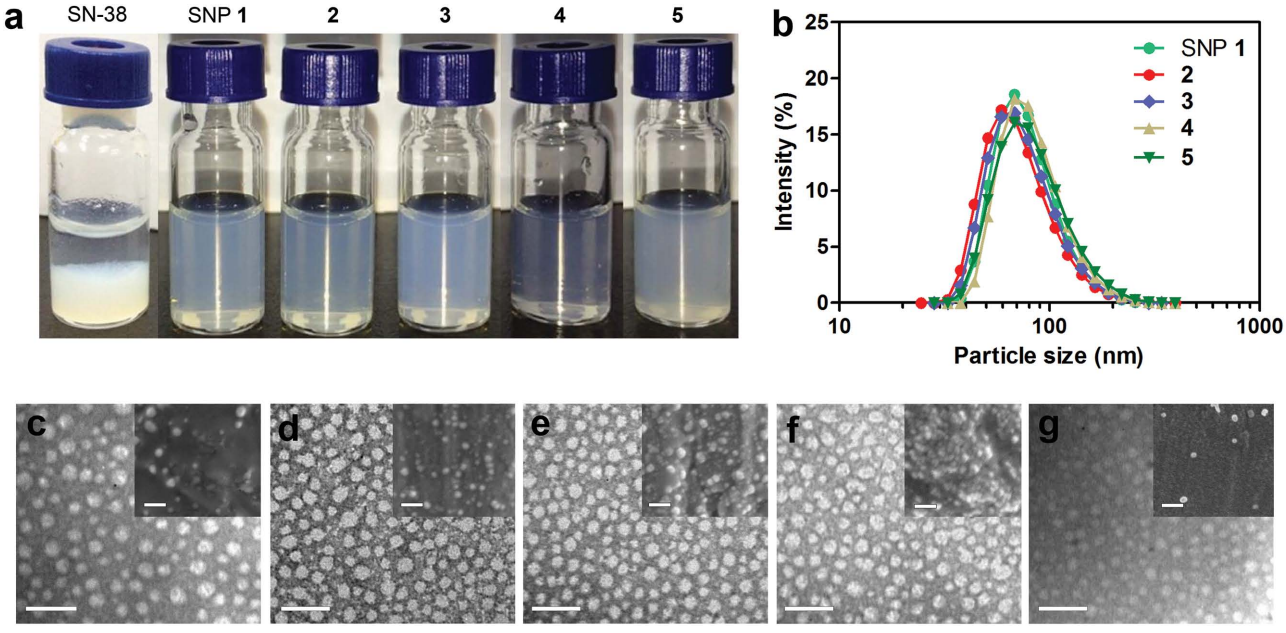

Figure 2. a) Prodrugs **1–5** (0.5 mg mL^{-1}) can dissolve in water to form clear and transparent solutions, but free SN-38 can precipitate. b) Size distribution and c–g) TEM images of assembled nanostructures for prodrugs **1–5**, respectively. Insets show SEM images. Scale bar, 100 nm.

hydrodynamic diameters (d_h) of ≈70 nm (Figure 2b). These DLS results are in accordance with the TEM images and the apparent enlargement should be attributed to a hydration layer. Remarkably, compared to previously reported squalenoylated drug conjugates,[14,15] the SN-38-based prodrugs produced much smaller particle sizes, suggesting that van der Waals attractions in addition to possible π–π stacking strongly constrained these amphiphiles together more tightly. Thus, we envisioned that these SNPs in the sub-100 nm range may have a substantial advantage in achieving favorable tumor penetration and the accumulation of active drugs.[32] The particle sizes are reproducible with this simple method under the current conditions, thus making SNP preparation robust enough for large-scale production. No tendency to form larger aggregates or precipitates was observed when the SNPs were stored at 4 °C for several weeks.

The potent antitumor compound SN-38 is highly hydrophobic and planar, leading to its total water insolubility. Previous efforts to increase solubility included modification of this potent agent with hydrophilic groups to induce the self-assembly into nanoparticles using SN-38 as the hydrophobic component.[16] Here, we extended the amphiphilic assembly concept to largely hydrophobic amphiphiles that are routinely unable to self-assemble in aqueous media. Notably, from the library of SN-38 prodrugs with structurally diverse modifications, we identified five prodrugs that are capable of spontaneously self-assembling into near-monodisperse SNPs that are well suited for the following intravenous administration. The self-assembly of molecular units into complicated and functional supramolecular architectures is ubiquitous in biological systems and synthetic chemistry.[33–35] Recently, such systems based on individual functionalized molecular building blocks have found a myriad of fascinating applications such as protein molecular sensing,[36–38] templated synthesis,[39] and amphiphilic polymer-based drug delivery[34] and have been used to create hierarchically functional structures.[40] However, the clinical use of self-assembling small-molecule prodrugs into stable suprastructures with favorable diameters, shapes, and pharmacokinetic properties has so far been an under-explored area of drug development.[14–17,41,42] The sole drugs commonly exhibit neither self-assembly nor stable aggregation under physiological conditions. Thus, in this study, to address these issues, we combined the drug reconstruction with the subsequent solution self-assembly strategy to promote the prodrug amphiphiles self-assembling in aqueous solutions.

2.3. Hydrolysis Kinetics of Prodrugs and Stability of SNPs

The structural integrity of prodrug-assembled nanoparticles in the bloodstream is necessary for tumor targeting via the EPR effect and could contribute to long-term circulation and subsequent antitumor activities. Therefore, we first used high-performance liquid chromatography (HPLC) analysis to compare the hydrolysis rates of prodrugs assembled in the form of nanostructures using **2** and **5** as model compounds at physiological pH (7.4) at 37 °C (**Figure 3**b). SNP **2** exhibited quite a slow degradation rate, with hydrolysis of ≈35% of the total amount of prodrug over 48 h. By contrast, a drastically distinct hydrolysis rate was observed for SNP **5**, in which 82% of the prodrug was hydrolyzed within 24 h. In our molecular design, lipophilicity was imparted to the SN-38 molecules to confer their self-assembly in aqueous solutions. However, this design

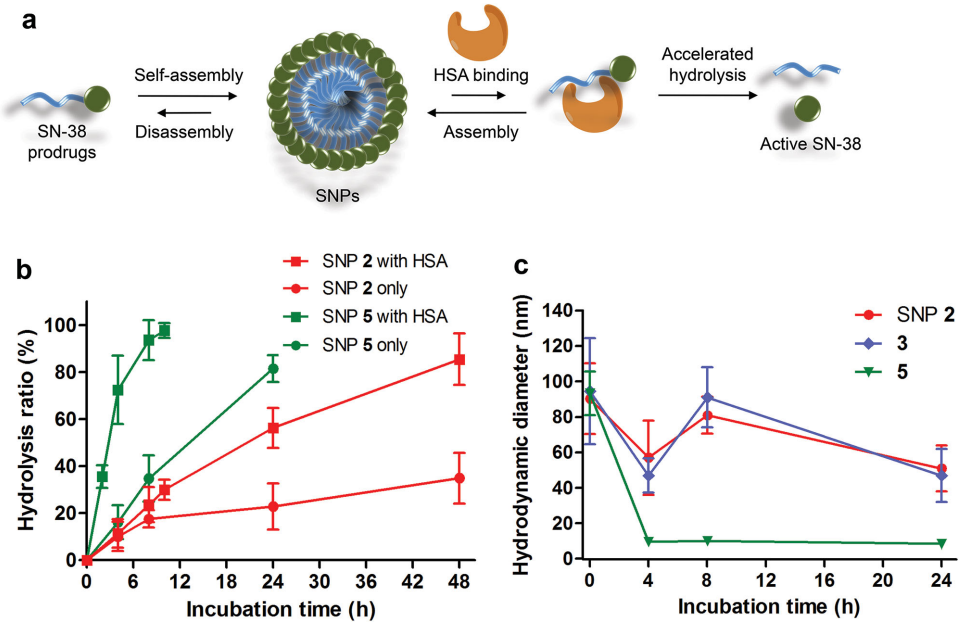

Figure 3. HSA can partially induce the disassembly of prodrugs by hydrophobic binding, accelerating their hydrolysis. a) A schematic illustration of this mechanism. b) Hydrolytic kinetics of SNPs **2** (red line) and **5** (green line) in the presence or absence of HSA (10 mg mL^{-1}). The samples were incubated in 50 × 10^{-3} M HEPES (4-(2-hydroxyethyl)-1-piperazineethanesulfonic acid) buffer (pH 7.4) at 37 °C. c) The hydrodynamic diameter profiles of SNPs **2**, **3**, and **5** (0.5 mg mL^{-1}, SN-38 equivalent) during incubation with 50% mouse serum. The data are presented as means ± SD (n = 3).

also made the prodrugs available for binding with endogenous human serum albumin (HSA),[43] which is abundant in blood. As depicted schematically in Figure 3a, this binding would lead to the disruption of the assembled nanostructures and accelerate the hydrolysis of prodrugs by disassembly-induced exposure of the phenyl ester bonds to an aqueous environment.[44] Thus, we further verified the hydrolytic kinetics of SNPs **2** and **5** in the presence of a high concentration of HSA (10 mg mL^{-1}). Inevitably, partial binding with HSA destabilized both SNPs **2** and **5**, sensitizing the prodrugs to hydrolysis; nevertheless, SNP **2** still exhibited robust resistance to hydrolysis for a relatively long time even in the presence of HSA (Figure 3b) due to the strong intermolecular forces conferred by modification with the polyunsaturated alkyl chain.

Next, the intactness of SNPs when incubated with excess amounts of HSA was directly assessed by TEM. Clearly, the morphology of SNP **2** appeared unchanged from that of the TEM images, whereas SNP **5** was consumed within 4 h. These results are in agreement with the hydrolytic studies (Figure S2, Supporting Information).

Finally, to confirm whether the SNPs can survive even in the presence of mouse serum, we used DLS measurements to investigate the stability of the prodrug-assembled SNPs. As shown in Figure 3c and Figure S3 (Supporting Information), when incubated with 50% mouse serum, the sizes of SNPs **2** and **3** remained unchanged over 24 h. However, SNP **5** can be disassembled in response to serum protein binding, resulting in the quick collapse of the nanostructures. These results are highly consistent with the evidence above, explicitly supporting the idea that prodrugs **1–3** can assemble into more stable suprastructures, which is likely due to the ability of polyunsaturated alkyl chains to adopt bent conformations and may also be caused by intermolecular π–π stacking. These results also excluded the possibility that the intact SNPs are rapidly disrupted by endogenous serum albumin in the blood after injection, and consequently, prodrugs are delivered by "hitchhiking" on albumin.[45] Thus, equilibrium towards the disassembly of SNPs **1–3** induced by albumin recognition would be significantly repressed in the presence of HSA, leading to the high stability of these nanoparticles. We could thus conclude that nanoprodrugs with highly stable characteristics are favored and may be delivered to the target tumor site via the EPR effect.

2.4. In Vitro Cytotoxicity and Apoptosis Assay Induced by Released SN-38

We next compared the in vitro cytotoxicity of SNPs **1–5** to CPT-11 and free SN-38 in three human cancer cell lines, namely the colon cancer lines HT-29 and HCT-116 and the nonsmall cell lung cancer line A549. After treatment for 48 or 72 h, the cell viability was measured using the standard MTT (3-(4,5-dimethylthiazol-2-yl)-2,5-diphenyl tetrazolium bromide) assay. The half-maximal inhibitory concentration (IC_{50}) values are summarized in Table S1 (Supporting Information). The SNPs composed of pure prodrugs **1–5** exerted far greater cytotoxic effects than CPT-11 in all tested cells, suggesting superior cytotoxicity of the reconstructed prodrugs over approved CPT-11 (**Figure 4**a and Figure S4, Supporting Information). Compared to free SN-38 after 48 h incubation, these SNPs **1–5** were less effective in killing cancer cells, likely due to the delayed release of the active SN-38 molecule. However, prolonged incubation (72 h) with these SNPs significantly reduced cell proliferation, and the IC_{50} values were comparable to those of free SN-38 (Figure 4b).

To confirm that the inhibition of cancer cells was a consequence of SN-38-induced apoptosis, fluorescence-activated cell sorting (FACS)-based analysis was performed. Both early and late apoptosis were determined using the Alexa Fluor 488 Annexin V/propidium iodide (PI) double-staining assay, which can specifically detect the exposure of phosphatidylserine, an essential event in apoptosis.[46] As expected, after treatments with SNPs **1–5**, apoptosis was detected in HT-29 cells (Figure 4c). Therefore, these SNPs can efficiently induce early and late apoptosis in a large population of cells after 48 h.

2.5. Comparison of Pharmacokinetics with Prodrug-Assembled SNPs

The in vivo antitumor efficacy greatly improves upon long-term circulation of prodrug-assembled SNPs, which also ultimately affect the accumulation of drugs in tumors via the EPR effect. As described previously, the structural variations of the modifications to SN-38 molecules significantly modulated the self-assembly of the prodrugs and, most likely, the disassembly induced by HSA binding. These modifications subsequently change the stability of SNPs when they contact the serum albumins that are abundant in blood. Thus, the blood circulation of SNPs **2**, **3**, and **5** was compared in Sprague Dawley (SD) rats (≈250 g) after a single intravenous (i.v.) administration of a 15 mg kg^{-1} SN-38 equivalent dose of SNPs. As shown in **Figure 5**, compared to the rapid clearance of SNP **5**, SNPs **2** and **3** clearly exhibited prolonged retention in the blood. The serum concentration of SN-38 in particular was maintained for up to 7 h when SNP **2** and **3** was used, giving a significantly higher area under the blood concentration curve (AUC_{0-7h}) compared to SNP **5** (51.0 and 32.7 vs 6.9 μg h mL^{-1}, $p < 0.01$, Table S2, Supporting Information). Our results clearly indicate that the prodrugs modified with flexible polyunsaturated fatty acids significantly prolong the drug presence in blood and that the structural stability of SNPs contributes favorably to in vivo pharmacokinetics.

The use of near-infrared (NIR) probes encapsulated in the assembled SNPs provides a convenient method for evaluating the blood retention time of nanoparticles. We therefore coassembled the hydrophobic DiR dye into the core of SNPs. After i.v. injection, the fluorescence signals derived from NIR probes in the whole body were monitored (Figure S5a, Supporting Information). As expected, the NIR signals in the mice injected with free DiR were eliminated rapidly from the body within several hours. By comparison, encapsulation of DiR in SNP **2** clearly led to strong and stable NIR fluorescence for up to 24 h. To further elucidate the in vivo biodistribution of DiR-loaded SNPs, ex vivo flurescence images of the mice tissues including tumors were examined. As shown in Figure S5b,c (Supporting Information), DiR probes encapsulated in the SNPs **2** and **5** exhibited the enhanced accumulation in tumors compared to free DiR, indicating that the SNP platform may help to deliver payloads to tumors via EPR

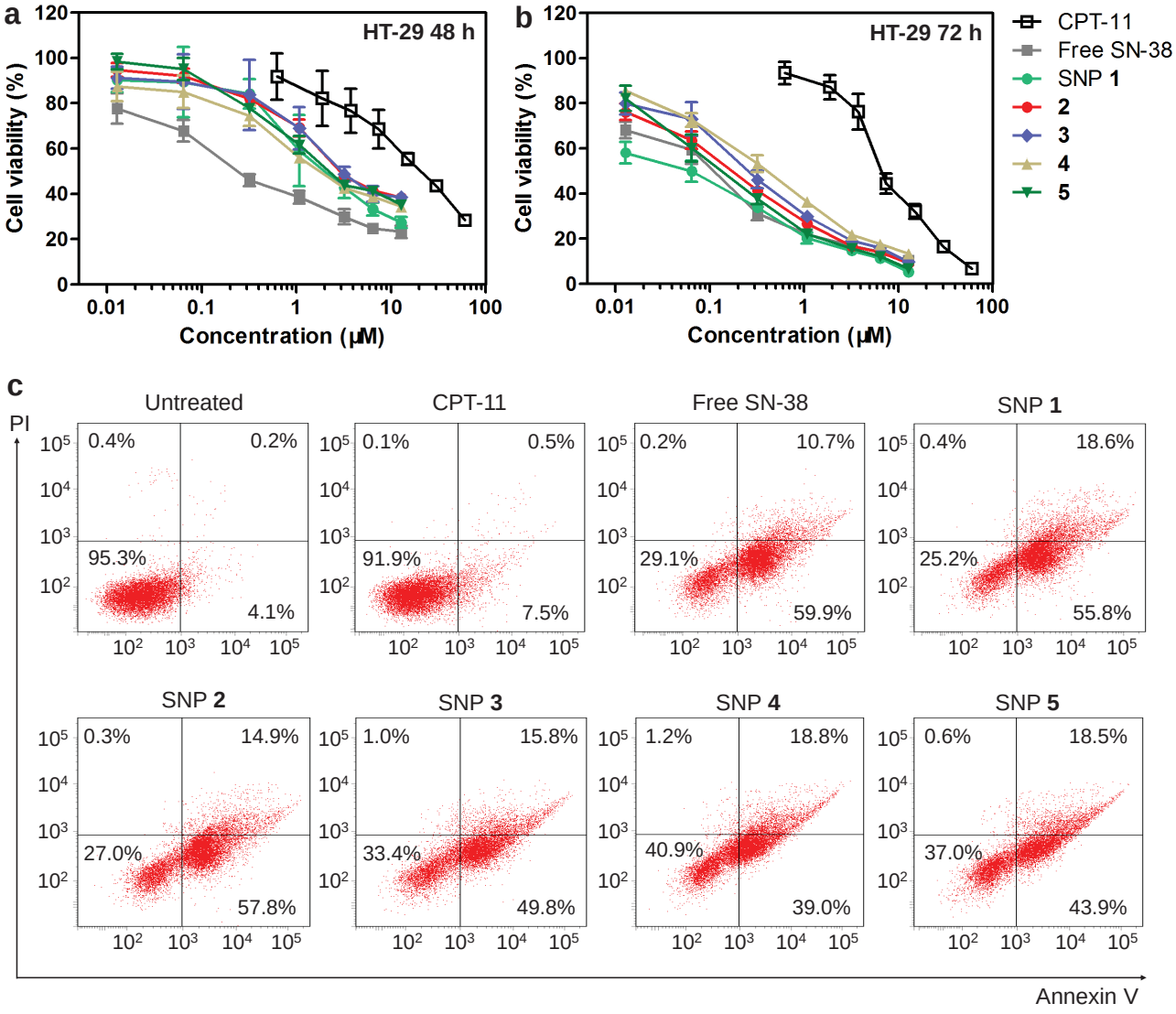

Figure 4. HT-29 cell viability after a) 48 h or b) 72 h treatment with CPT-11, free SN-38, and SNPs **1–5** as determined using the MTT assay. c) HT-29 cell apoptosis was determined by FACS using the Alexa Fluor 488 Annexin V/PI staining kit after 48 h drug treatments. Four distinct phenotypes were observed: viable cells (lower left quadrant); early apoptotic cells (lower right quadrant); late apoptotic cells (upper right quadrant); necrotic or dead cells (upper left quadrant).

effect. In addition, DiR probes in SNP **2** showed higher uptake in tumor tissue than that in SNP **5**. We also observed strong fluorescence intensity in the liver and spleen. This might attribute to the leakage of SNP-encapsulated DiR probes when circulating in blood stream because they are noncovalently trapped. Taken together, these results are consistent with the in vitro stability and the pharmacokinetic studies described above, demonstrating that the enhanced stability conferred by prodrug **2** promoted the retention of NIR probes in the mouse body and consequently contributed to higher intratumoral accumulation.

2.6. In Vivo Antitumor Efficacy of SNPs in Solid Tumors

Due to their spontaneous assembly into nanoparticles in aqueous solutions, the optimized SNPs **1–5** are expected to be

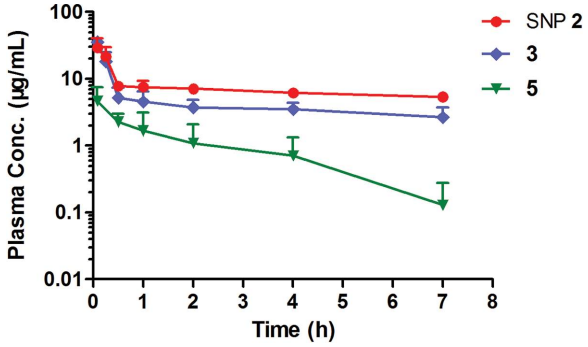

Figure 5. In vivo plasma concentration-time profile of SN-38 prodrug **2**, **3**, and **5**-assembled SNPs following i.v. administration at doses of 15 mg kg^{-1} (SN-38 equivalent) to SD rats. The total SN-38 in the plasma was extracted and analyzed by HPLC. The data are presented as means ± SD ($n = 4$).

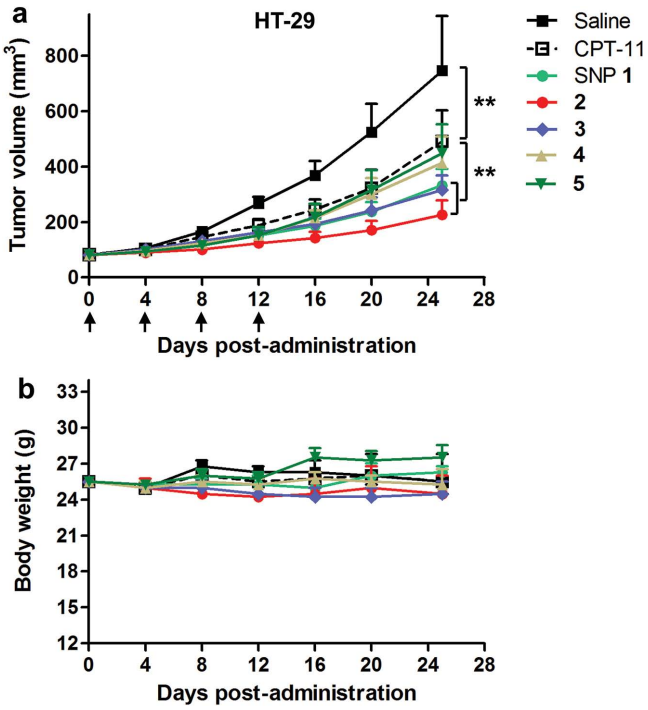

Figure 6. In vivo antitumor activity of SN-38 prodrug-assembled SNPs. a) Tumor growth and b) body-weight changes of mice bearing HT-29 tumor xenografts. All groups ($n = 7$) of mice were intravenously injected with SNPs (20 mg kg^{-1}, SN-38 equivalent) dissolved in saline on day 0, 4, 8, and 12. CPT-11 (23 mg kg^{-1}) was administered intravenously as the control. The data are reported as means ± SD, $^{**}p < 0.01$.

compatible with parenteral administration. To translate them for potential therapeutic utility, the in vivo antitumor activity was initially evaluated in nude mice bearing subcutaneously grafted human colon HT-29 tumors. When the tumors reached an average volume of 80 mm^3, SNPs **1–5** were intravenously injected four times on days 0, 4, 8, and 12, and the tumor growth was followed for up to 25 d as shown in **Figure 6**a. CPT-11, a standard-of-care drug for colon cancers, only reduced the volume of HT-29 tumors by 38% ($p < 0.01$). Meanwhile, SNPs **1–3** significantly retarded the tumor progression. In particular, mice treated with SNP **2** exhibited more drastic tumor growth inhibition of 78% at day 25. By comparison, SNPs **4** and **5**, in which the phenolate group of SN-38 is modified by less lipophilic amino acids, showed antitumor efficacy that was similar to that of CPT-11 ($p > 0.05$). In an additional experiment using a xenograft model of human nonsmall cell lung A549 solid tumors, a similar pattern in tumor growth inhibition was observed with these SNPs (Figure S6, Supporting Information).

Importantly, the body weights of mice receiving successive treatments remained stable in both antitumor experiments (Figure 6b and Figure S6, Supporting Information). Moreover, the mice injected with an elevated dose of 30 mg kg^{-1} (SN-38 equivalent) did not present changes in body weights (data not shown), indicating a low systemic toxicity associated with the present SN-38 prodrug-assembled SNPs.

2.7. Improving the Efficacy of SNP by Integration of Tumor-Specific Peptidic Ligand

The favorable stability of nanoparticles derived from prodrugs **1**, **2**, and **3** makes them promising candidates for further clinical evaluation. Although nanoprodrugs based on the SN-38 dimers have been recently reported,[30] our results demonstrated that polyunsaturated alkyl chain-based modifiers can greatly improve the stability of generated nanoarchitectures and subsequently confer excellent antitumor efficacy. Due to the modular feature of this SNP fabrication strategy, it can be envisaged that additional valuable functionalities such as tumor-specific ligands can be integrated onto the surfaces of the nanoplatforms by coassembly (**Figure 7**a), which could further improve the potential of these nanoassemblies as a practical therapeutic modality.[47–49]

As a proof-of-concept, we used a recently discovered cyclic peptide ligand, iRGD (CRGDK/RGPD/EC), to specifically deliver SNPs to tumor sites.[50,51] To accomplish this, the iRGD motif with a reactive cysteine residue was used to conjugate with hydrophobic linoleic acid via the maleimide–thiol coupling (Figure 7b). Because the iRGD moiety possesses high hydrophilicity, it can be rationally expected that the amphiphilic construct **27** is capable of coassembling with SN-38 prodrug **2** to generate iRGD-decorated SNP **2** (termed iSNP **2**), thereby facilitating the ligand displayed on the particle surface. In vitro data clearly showed that the spherical nanoparticulate morphology was formed and the particle size was similar with SNP **2** irrespective of adding the peptidic ligand (Figure 7c,d). To further investigate the therapeutic activity of iSNP **2**, A549 tumor-bearing mice were i.v. injected with SNP **2** and iSNP **2** at different dose levels (20 and 30 mg kg^{-1}, respectively). Clearly, the targetable iSNP **2** with iRGD decorated outperformed SNP **2** in reducing tumor regression at both dose levels ($p < 0.05$), suggesting that incorporation of the tumor-specific ligand might help improve the performance of our SN-38-based nanoprodrugs (Figure 7e).

3. Conclusion

Based on the premise that the freely polar hydroxyl group on the SN-38 prodrug serves as a solvophilic moiety, we have successfully reconstructed and optimized robust water-soluble supramolecular nanoprodrugs **1–3**, which are suitable for in vivo administration. Reliance on van der Waals attractions and strong π–π interactions, as well as the high structural flexibility of modifiers, endowed this solvent- and adjuvant-free delivery platform with enough stability to survive in the blood, thereby allowing delivery of the drugs to target tumor site(s) via EPR effects. The platforms presented here have notable advantages over their existing polymer-based counterparts in terms of ease of chemical synthesis, economical fabrication, and bulk scale of production. To the best of our knowledge, this study is the first in-depth investigation of how structural variations in small-molecule prodrugs correlate with their in vivo antitumor activity. Thus, our results also provided novel mechanistic insights into the principles of rational prodrug design and might open new

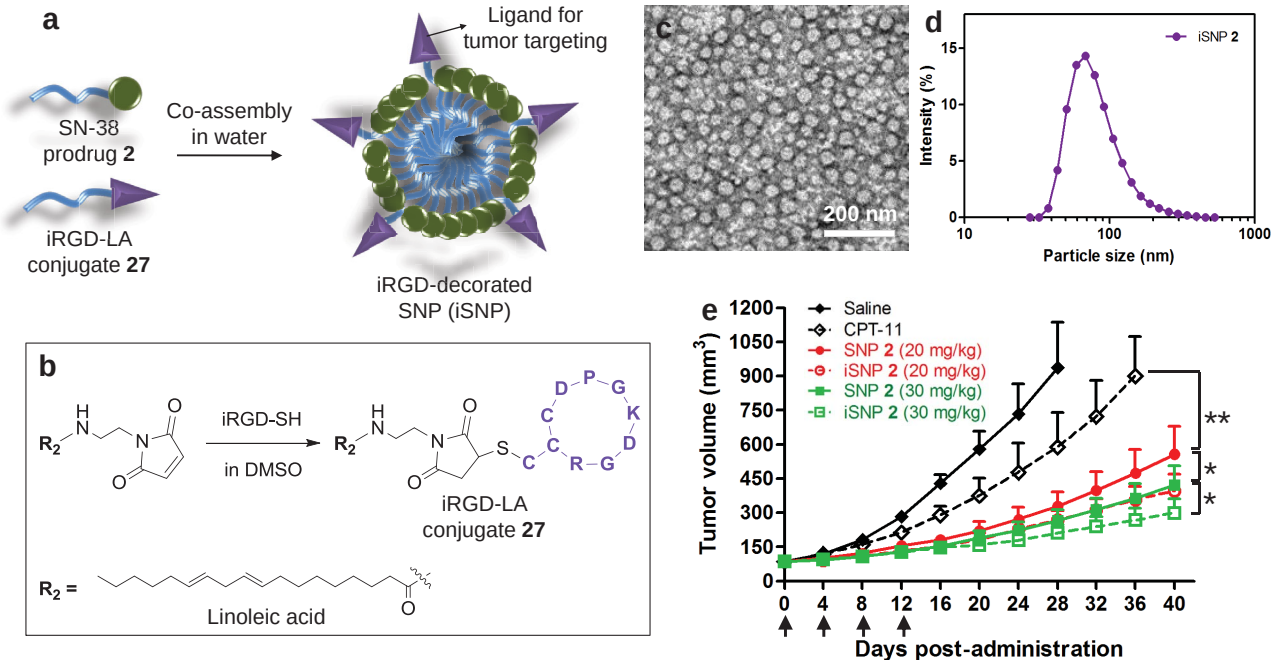

Figure 7. Improving in vivo antitumor activity of SNP **2** by incorporation of a tumor-specific targeting ligand, iRGD. a) Schematic illustration of combination of prodrug **2** with iRGD-modified linoleic acid **27** for fabrication of targetable nanoprodrug. b) Molecular structure and synthesis of conjugate **27**. Cyclic iRGD motif is shown in purple. c) TEM image and d) size distribution of iSNP **2**. e) Tumor growth of mice bearing A549 tumor xenografts. All groups ($n = 7$) of mice were intravenously injected with various SNP formulations (SN-38 equivalent) dissolved in saline on day 0, 4, 8, and 12. Saline and CPT-11 (23 mg kg^{-1}) were administered intravenously as the control. The data are reported as means ± SD, $*p < 0.05$, $**p < 0.01$.

opportunities for using these stable nanoprodrugs as practical and valuable antitumoral platforms.

4. Experimental Section

Materials: 7-Ethyl-10-hydroxycamptothecin (SN-38) was purchased from Knowshine Pharmachemicals Inc. (Shanghai, China). Cyclic iRGD (CRGDKGPDC)C-SH was customized by GL Biochem Ltd. (Shanghai, China). MTT was purchased from Aladdin (Shanghai, China). Alexa Fluor 488 Annexin V/PI apoptosis assay kit, DiR (D12731) probe and cell culture reagents were purchased from Life Technologies (Shanghai, China). All other compounds and solvents were purchased from J&K Chemical (Shanghai, China).

Assessment of SN-38 Prodrugs for Self-Assembly in Aqueous Solution: Prodrugs were dissolved in DMSO (20 mg mL^{-1}) and then rapidly injected into ddH_2O at a final concentration of 2 mg mL^{-1} prodrug to observe their solubility. The solutions were further dialyzed using ddH_2O to remove the organic solvent. This procedure enabled the identification of five prodrugs that are capable of forming transparent solutions at concentrations greater than 2 mg mL^{-1}.

Preparation of iRGD-Decorated SNP **2**: Prodrug **2** and iRGD-conjugated LA **27** were dissolved in DMSO in a molar ratio with 10:1 and injected into ddH_2O to form nanoprecipitation. For i.v. injection, the solutions were further dialyzed using ddH_2O to remove the organic solvent and the drug concentration was determined by HPLC analysis.

TEM and SEM Analysis: The TEM samples were prepared by dipping SNPs **1–5** (0.5 mg mL^{-1} prodrug) onto a 300-mesh copper grid coated with carbon. A few minutes after deposition, the surface water was removed with filter paper, and then the samples were dried at room temperature. Positive staining was performed using a 2 wt% aqueous uranyl acetate solution followed by air drying. TECNAL 10 (Philips) was used to obtain TEM images, operating at an acceleration voltage of 80 kV. The morphology of SNP **1–5** was observed in a Hitachi SU-70 thermal field emission scanning electron microscope (FE-SEM).

DLS Measurement: The hydrodynamic diameters of SNPs **1–5** were analyzed by DLS (Malvern Nano-S90, UK).

HPLC Determination of Hydrolysis Rates of Prodrug-Assembled SNPs: The in vitro hydrolysis of the SN-38 prodrugs in the presence or absence of HSA was evaluated by HPLC analysis. Briefly, 10 mL aqueous solutions of SNPs **2** and **5** (0.1 mg mL^{-1}) were incubated with or without HSA (10 mg mL^{-1}) at 37 °C. At various time intervals, aliquot samples (0.5 mL) were collected and subjected to HPLC at a flow rate of 1.0 mL min^{-1} using a gradient of 20%–100% acetonitrile in water the as mobile phase. To assay the free SN-38 and intact prodrug content, UV detection at a wavelength of 378 nm and a C18 ODS reverse-phase column (5 μm, 250 mm × 4.6 mm, YMC Co., Ltd., Kyoto, Japan) were utilized. The hydrolysis rate of the prodrugs was calculated as a function of the incubation time.

Stability of Prodrug Self-Assembled Nanoparticles: SNPs in ddH_2O (0.5 mg mL^{-1}, SN-38 equivalent) were added to a solution containing HSA (20 mg mL^{-1}). The samples were incubated at 37 °C for an extended period of time, and the morphology of SNPs was observed by TEM as described previously. In addition, for DLS measurements, the SNPs containing prodrugs (0.5 mg mL^{-1}, SN-38 equivalent) were mixed with mouse serum.

In Vitro Cytotoxicity Assay: The cytotoxicities of SNPs **1–5** against human tumor cell lines, including human colon cancer (HT-29 and HCT-116) and nonsmall cell lung cancer (A549), were determined using the MTT assay. Briefly, the cells were plated in 96-well plates (5000 cells well^{-1}) and incubated at 37 °C for 24 h. Serial dilutions of CPT-11, free SN-38 or SNPs were added to the cells before further incubation for 48 or 72 h. Subsequently, 30 μL MTT solution (5 mg mL^{-1}) was added to each well. The plates were incubated at 37 °C and 5% CO_2 for 4 h, allowing viable cells to reduce the yellow tetrazolium salt into dark blue formazan crystals. After the addition of DMSO (100 μL), the

absorbance at 490 nm was determined using a SynergyHT plate reader (BioTek, Winooski, VT, USA).

Apoptosis Analysis by Flow Cytometry: HT-29 cells were seeded at a density of 1×10^6 cells mL^{-1} in each well and allowed to grow overnight. Then, the cells were incubated with CPT-11 (1×10^{-6} M), SN-38 (1×10^{-6} M), or SNPs **1–5** (1×10^{-6} M, SN-38 equivalent) for 48 h at 37 °C. The cells without drug treatment were used as a control. Cells were recovered and washed with cold phosphate buffered saline (PBS) repeatedly. For apoptosis analysis, an Alexa Fluor 488 annexin V/PI apoptosis detection kit was used according to the manufacturer's protocol. Briefly, treated and untreated cells (1×10^5) were suspended in 1× annexin V binding buffer (100 µL) (10×10^{-3} M HEPES, 140×10^{-3} M NaCl, and 2.5×10^{-3} M CaCl2, pH 7.4), followed by addition of 5 µL Alexa Fluor 488 annexin V and 1 µL PI (100 µg mL^{-1}) to each sample. The cells then were incubated at room temperature for 15 min and binding buffer (400 µL) was added while gently mixing. The stained cells were analyzed directly using a BD FACSCantoTM II flow cytometer.

Animal Studies: All animals received care in compliance with the guidelines outlined in the Guide for the Care and Use of Laboratory Animals. They were housed under aseptic conditions and given an autoclaved rodent diet and sterile water. The animal experiments were approved by the Animal Care and Use Committee of Zhejiang University.

In Vivo Pharmacokinetic Properties of SNPs: SD rats ($n = 4$ for each group) were used to assess the blood circulation of SNPs. The animals were administered SNPs **2**, **3**, and **5** intravenously at a dose equivalent to 15 mg kg^{-1} of SN-38. Blood samples were collected in microtubes, and plasma was harvested at 5, 15, and 30 min and 1, 2, 4, and 7 h postapplication. The plasma samples were stored at −20 °C until analysis. The concentrations of SN-38 including free SN-38 and prodrugs from the plasma samples were measured by HPLC. The data were fitted to a two compartment pharmacokinetic model.

In Vivo NIR Imaging: The NIR fluorescence dye DiR was coassembled with prodrugs **2** and **5** by injection of the mixture of DiR and prodrugs in DMSO into PBS. A noninvasive optical imaging system was utilized. When the tumor volume reached ≈200 mm^3, mice were injected with free DiR (1.2 mg kg^{-1}) as the control and SNPs **2** and **5** containing DiR (1.2 mg kg^{-1}) via the tail vein. NIR fluorescence imaging was performed at 2, 4, 8, 12, and 24 h postinjection using the Maestro in vivo imaging system. For ex vivo flurescence imaging, organs (heart, liver, spleen, lung, and kidney) and tumors were harvested and imaged immediately.

*In Vivo Antitumor Activity of SNPs***1–5**: HT-29 (human colon cancer cells) and A549 (human nonsmall cell lung cancer cells) tumors were harvested from subcutaneously growing tumors in nude mice hosts and implanted subcutaneously into the right flank of 5-week-old BALB/c nude mice (Shanghai Experimental Animal Center, Chinese Academy of Science). When the tumors reached an average volume of 80 mm^3, the animals were assigned for treatment (day 0). The mice were given intravenous injections of SNPs or iSNP four times on days 0, 4, 8, and 12 at a dose equivalent to 20 or 30 mg kg^{-1} of SN-38. Control mice were injected with saline and 23 mg kg^{-1} Irinotecan (CPT-11) following the same schedule. The tumor growth and body weight were monitored and recorded at predetermined time intervals. The tumor volume was calculated according to the following formula: $V = (L \times W^2)/2$, where L and W were the greatest length and widest diameter of tumors, respectively.

Statistical Analysis: All quantitative data are presented as the means ± SD of three independent experiments. The significance of compared measurements was evaluated using a two-tailed unpaired Student's *t*-test. A *p*-value of less than 0.05 was considered significant, while a *p*-value of less than 0.01 was considered highly significant.

Supporting Information

Supporting Information is available from the Wiley Online Library or from the author.

Acknowledgements

This work was supported by the Chinese High Tech Research and Development (863) Program (2012AA020204), the National Natural Science Foundation of China (21202147, 81421062, and 81272675), the National S&T Major Project (2012ZX10002017 and 2012ZX10002010-001-005), the Major Science and Technology Project of Zhejiang Province (2014C03043-2), and the Natural Science Foundation of Zhejiang Province (LY13H160004 and LY13H090013).

Received: May 12, 2015
Revised: June 9, 2015
Published online: July 6, 2015

[1] R. A. Petros, J. M. DeSimone, *Nat. Rev. Drug Discovery* **2010**, *9*, 615.
[2] N. Kamaly, Z. Xiao, P. M. Valencia, A. F. Radovic-Moreno, O. C. Farokhzad, *Chem. Soc. Rev.* **2012**, *41*, 2971.
[3] a) K. Riehemann, S. W. Schneider, T. A. Luger, B. Godin, M. Ferrari, H. Fuchs, *Angew. Chem. Int. Ed.* **2009**, *48*, 872; b) K. Riehemann, S. W. Schneider, T. A. Luger, B. Godin, M. Ferrari, H. Fuchs, *Angew. Chem.* **2009**, *121*, 886.
[4] H. Maeda, J. Wu, T. Sawa, Y. Matsumura, K. Hori, *J. Controlled Release* **2000**, *65*, 271.
[5] S. Dhar, N. Kolishetti, S. J. Lippard, O. C. Farokhzad, *Proc. Natl. Acad. Sci. U.S.A.* **2011**, *108*, 1850.
[6] H. Cabral, M. Murakami, H. Hojo, Y. Terada, M. R. Kano, U. I. Chung, N. Nishiyama, K. Kataoka, *Proc. Natl. Acad. Sci. U.S.A.* **2013**, *110*, 11397.
[7] J. Hrkach, D. Von Hoff, M. Mukkaram Ali, E. Andrianova, J. Auer, T. Campbell, D. De Witt, M. Figa, M. Figueiredo, A. Horhota, S. Low, K. McDonnell, E. Peeke, B. Retnarajan, A. Sabnis, E. Schnipper, J. J. Song, Y. H. Song, J. Summa, D. Tompsett, G. Troiano, T. Van Geen Hoven, J. Wright, P. LoRusso, P. W. Kantoff, N. H. Bander, C. Sweeney, O. C. Farokhzad, R. Langer, S. Zale, *Sci. Transl. Med.* **2012**, *4*, 128ra39.
[8] C. Jiang, H. Wang, X. Zhang, Z. Sun, F. Wang, J. Cheng, H. Xie, B. Yu, L. Zhou, *Int. J. Pharm.* **2014**, *475*, 60.
[9] J. Cui, Y. Yan, Y. Wang, F. Caruso, *Adv. Funct. Mater.* **2012**, *22*, 4718.
[10] a) Z. Zhou, X. Ma, C. J. Murphy, E. Jin, Q. Sun, Y. Shen, E. A. Van Kirk, W. J. Murdoch, *Angew. Chem. Int. Ed.* **2014**, *53*, 10949; b) Z. Zhou, X. Ma, C. J. Murphy, E. Jin, Q. Sun, Y. Shen, E. A. Van Kirk, W. J. Murdoch, *Angew. Chem.* **2014**, *126*, 11129.
[11] D. Ma, G. Hettiarachchi, D. Nguyen, B. Zhang, J. B. Wittenberg, P. Y. Zavalij, V. Briken, L. Isaacs, *Nat. Chem.* **2012**, *4*, 503.
[12] Y. Yang, R. M. Pearson, O. Lee, C.-W. Lee, R. T. Chatterton Jr., S. A. Khan, S. Hong, *Adv. Funct. Mater.* **2014**, *24*, 2442.
[13] H. Cabral, K. Kataoka, *J. Controlled Release* **2014**, *190*, 465.
[14] P. Couvreur, B. Stella, L. H. Reddy, H. Hillaireau, C. Dubernet, D. Desmaele, S. Lepetre-Mouelhi, F. Rocco, N. Dereuddre-Bosquet, P. Clayette, V. Rosilio, V. Marsaud, J. M. Renoir, L. Cattel, *Nano Lett.* **2006**, *6*, 2544.
[15] A. Maksimenko, F. Dosio, J. Mougin, A. Ferrero, S. Wack, L. H. Reddy, A. A. Weyn, E. Lepeltier, C. Bourgaux, B. Stella, L. Cattel, P. Couvreur, *Proc. Natl. Acad. Sci. U.S.A.* **2014**, *111*, E217.
[16] Y. Shen, E. Jin, B. Zhang, C. J. Murphy, M. Sui, J. Zhao, J. Wang, J. Tang, M. Fan, E. Van Kirk, W. J. Murdoch, *J. Am. Chem. Soc.* **2010**, *132*, 4259.
[17] Z. Zhou, X. Ma, E. Jin, J. Tang, M. Sui, Y. Shen, E. A. Van Kirk, W. J. Murdoch, M. Radosz, *Biomaterials* **2013**, *34*, 5722.
[18] P. Gou, W. Liu, W. Mao, J. Tang, Y. Shen, M. Sui, *J. Mater. Chem. B* **2013**, *1*, 284.
[19] a) T. Sun, Y. S. Zhang, B. Pang, D. C. Hyun, M. Yang, Y. Xia, *Angew. Chem. Int. Ed.* **2014**, *53*, 12320; b) T. Sun, Y. S. Zhang, B. Pang, D. C. Hyun, M. Yang, Y. Xia, *Angew. Chem.* **2014**, *126*, 12520.

[20] S. Mura, J. Nicolas, P. Couvreur, *Nat. Mater.* **2013**, *12*, 991.
[21] Y. Wang, M. S. Shim, N. S. Levinson, H.-W. Sung, Y. Xia, *Adv. Funct. Mater.* **2014**, *24*, 4206.
[22] A. G. Cheetham, P. Zhang, Y. A. Lin, L. L. Lock, H. Cui, *J. Am. Chem. Soc.* **2013**, *135*, 2907.
[23] Y. Pommier, *Nat. Rev. Cancer* **2006**, *6*, 789.
[24] J. G. Slatter, L. J. Schaaf, J. P. Sams, K. L. Feenstra, M. G. Johnson, P. A. Bombardt, K. S. Cathcart, M. T. Verburg, L. K. Pearson, L. D. Compton, L. L. Miller, D. S. Baker, C. V. Pesheck, R. S. Lord, *Drug Metab. Dispos.* **2000**, *28*, 423.
[25] B. D. Wallace, H. Wang, K. T. Lane, J. E. Scott, J. Orans, J. S. Koo, M. Venkatesh, C. Jobin, L. A. Yeh, S. Mani, M. R. Redinbo, *Science* **2010**, *330*, 831.
[26] a) H. Wang, H. Xie, J. Wu, X. Wei, L. Zhou, X. Xu, S. Zheng, *Angew. Chem. Int. Ed.* **2014**, *53*, 11532; b) H. Wang, H. Xie, J. Wu, X. Wei, L. Zhou, X. Xu, S. Zheng, *Angew. Chem.* **2014**, *126*, 11716.
[27] M. C. Parrott, M. Finniss, J. C. Luft, A. Pandya, A. Gullapalli, M. E. Napier, J. M. DeSimone, *J. Am. Chem. Soc.* **2012**, *134*, 7978.
[28] K. S. Chu, M. C. Finniss, A. N. Schorzman, J. L. Kuijer, J. C. Luft, C. J. Bowerman, M. E. Napier, Z. A. Haroon, W. C. Zamboni, J. M. DeSimone, *Nano Lett.* **2014**, *14*, 1472.
[29] K. Baba, H. Kasai, A. Masuhara, H. Oikawa, H. Nakanishi, *Jpn. J. Appl. Phys.* **2009**, *48*, 117002.
[30] a) H. Kasai, T. Murakami, Y. Ikuta, Y. Koseki, K. Baba, H. Oikawa, H. Nakanishi, M. Okada, M. Shoji, M. Ueda, H. Imahori, M. Hashida, *Angew. Chem. Int. Ed.* **2012**, *51*, 10315; b) H. Kasai, T. Murakami, Y. Ikuta, Y. Koseki, K. Baba, H. Oikawa, H. Nakanishi, M. Okada, M. Shoji, M. Ueda, H. Imahori, M. Hashida, *Angew. Chem.* **2012**, *124*, 10461.
[31] M. Pinot, S. Vanni, S. Pagnotta, S. Lacas-Gervais, L. A. Payet, T. Ferreira, R. Gautier, B. Goud, B. Antonny, H. Barelli, *Science* **2014**, *345*, 693.
[32] H. Cabral, Y. Matsumoto, K. Mizuno, Q. Chen, M. Murakami, M. Kimura, Y. Terada, M. R. Kano, K. Miyazono, M. Uesaka, N. Nishiyama, K. Kataoka, *Nat. Nanotechnol.* **2011**, *6*, 815.
[33] G. M. Whitesides, B. Grzybowski, *Science*, **2002**, *295*, 2418.
[34] H. Cabral, N. Nishiyama, K. Kataoka, *Acc. Chem. Res.* **2011**, *44*, 999.
[35] C. Wang, Z. Wang, X. Zhang, *Acc. Chem. Res.* **2012**, *45*, 608.
[36] Y. Takaoka, T. Sakamoto, S. Tsukiji, M. Narazaki, T. Matsuda, H. Tochio, M. Shirakawa, I. Hamachi, *Nat. Chem.* **2009**, *1*, 557.
[37] Y. Takaoka, K. Kiminami, K. Mizusawa, K. Matsuo, M. Narazaki, T. Matsuda, I. Hamachi, *J. Am. Chem. Soc.* **2011**, *133*, 11725.
[38] K. Mizusawa, Y. Takaoka, I. Hamachi, *J. Am. Chem. Soc.* **2012**, *134*, 13386.
[39] a) F. Nudelman, N. A. Sommerdijk, *Angew. Chem. Int. Ed.* **2012**, *51*, 6582; b) F. Nudelman, N. A. Sommerdijk, *Angew. Chem.* **2012**, *124*, 6686.
[40] T. Aida, E. W. Meijer, S. I. Stupp, *Science* **2012**, *335*, 813.
[41] Y. Wang, D. Liu, Q. Zheng, Q. Zhao, H. Zhang, Y. Ma, J. K. Fallon, Q. Fu, M. T. Haynes, G. Lin, R. Zhang, D. Wang, X. Yang, L. Zhao, Z. He, F. Liu, *Nano Lett.* **2014**, *14*, 5577.
[42] P. Huang, D. Wang, Y. Su, W. Huang, Y. Zhou, D. Cui, X. Zhu, D. Yan, *J. Am. Chem. Soc.* **2014**, *136*, 11748.
[43] Y. R. Zheng, K. Suntharalingam, T. C. Johnstone, H. Yoo, W. Lin, J. G. Brooks, S. J. Lippard, *J. Am. Chem. Soc.* **2014**, *136*, 8790.
[44] D. A. Torres, M. Garzoni, A. V. Subrahmanyam, G. M. Pavan, S. Thayumanavan, *J. Am. Chem. Soc.* **2014**, *136*, 5385.
[45] H. Liu, K. D. Moynihan, Y. Zheng, G. L. Szeto, A. V. Li, B. Huang, D. S. Van Egeren, C. Park, D. J. Irvine, *Nature* **2014**, *507*, 519.
[46] S. E. Logue, M. Elgendy, S. J. Martin, *Nat. Protoc.* **2009**, *4*, 1383.
[47] H. Wang, W. Chen, H. Xie, X. Wei, S. Yin, L. Zhou, X. Xu, S. Zheng, *Chem. Commun.* **2014**, *50*, 7806.
[48] E. Ruoslahti, *Adv. Mater.* **2012**, *24*, 3747.
[49] Y. Zhong, F. Meng, C. Deng, Z. Zhong, *Biomacromolecules* **2014**, *15*, 1955.
[50] K. N. Sugahara, T. Teesalu, P. P. Karmali, V. R. Kotamraju, L. Agemy, O. M. Girard, D. Hanahan, R. F. Mattrey, E. Ruoslahti, *Cancer Cell* **2009**, *16*, 510.
[51] S. Su, H. Wang, X. Liu, Y. Wu, G. Nie, *Biomaterials* **2013**, *34*, 3523.